Kinetics of vanillin hydrodeoxygenation reaction in an organic solvent using a Pd/C catalyst

Aliu, Elias; Hart, Abarasi; Wood, Joe

Kinetics of Vanillin Hydrodeoxygenation Reaction in an Organic Solvent using Pd/C catalyst

Elias Aliu, Abarasi Hart, Joseph Wood *

School of Chemical Engineering, University of Birmingham, Edgbaston, Birmingham B15 2TT,

UK. *Corresponding Author: Tel: +44 (0) 121 414 5295. Email: j.wood@bham.ac.uk

ABSTRACT: In this work, the kinetics of vanillin (VL) hydrodeoxygenation (HDO) reaction to creosol (CR) over a 10% Pd/C catalyst were studied in a batch autoclave operated at 318 - 338K, 1-3MPa H_2 gas partial pressure, 35-65mM initial VL concentration ($C_{VL,0}$) and 0.13-0.27kg/m^3 catalyst loading. Experiments were carried out under negligible mass transfer interference which was verified by estimating the observable modulus, minimum stirring speed and maximum particle size. Additionally, the extent to which the products and acetic acid influences the reaction was examined. Two plausible Langmuir-Hinshelwood-Hougen-Watson (LHHW) models, competitive (Model I) and non-competitive (Model II) dissociative H_2 adsorption were discriminated using criteria that R^2 value greater than 99% indicates adequate fit to the experimental data. Model I emerged as the best fit with an R^2 value greater than 99%. The estimated activation energy was 50.6 kJ/mol, enthalpy of adsorption for H_2 28.9 kJ/mol and VL 32.5 kJ/mol.

1. INTRODUCTION

19   Fuels derived from fossil sources have long been the largest contributor to the global energy

20   supply chain. However, the surge in global energy consumption, perpetual decline in reserves

21   responsible for producing fossil fuels and increased awareness of their adverse effect on the

22   environment intensifies the need for alternative energy sources.[1,2] Future energy sources that are

23   both renewable and sustainable such as wind, solar and biomass are required. Bio-oils derived

24   from biomass represent a leading candidate among the possible alternative renewable and

25   sustainable fuels[3-5], owing to their ability to be used as drop-in fuels for existing vehicles and

26   potential to replace fossil derived feedstocks in chemical manufacture. The most recognised

27   technology for transforming biomass into bio-oil, known as fast pyrolysis, involves rapid heating

28   of the biomass particles under anaerobic condition and high temperature.[6-9]

29   Though the composition of bio-oil produced via fast pyrolysis varies with the biomass feedstock,

30   in general it contains a large amount of thermally and chemically unstable oxygenated compounds

31   such as aldehydes, ketones, acids, guaiacols, syringols etc.[10-13] The negative implications these

32   oxygenated compounds have on bio-oil physical properties include high viscosity, lower calorific

33   value, poor volatility and difficult storage due to high corrosiveness.[14-18] Hence, bio-oils must be

34   upgraded to fulfil their potential as both a substitute fuel and valuable chemical feedstock for

35   additional processes. Approaches under consideration for this purpose include aqueous phase

36   reforming, zeolite cracking and hydrotreating.[19-27]

37   Hydrotreating is the preferred approach because it ensures higher selectivity to liquid products,

38   and minimizes coke and gas formation.[28-30] Besides, it is a well-known process used in the

39   petroleum industry to remove heteroatoms such as sulphur, nitrogen and oxygen. In particular,

40   hydrodeoxygenation (HDO) which is one of the hydrotreating techniques is widely perceived as

41   the most economical route for upgrading bio-oil. Through HDO, the fuel quality of bio-oil

42 improves as a result of reduction in O: C ratio and increase in H: C ratio.[31-33] However, scale-up

43 of the HDO process has been limited by the lack of kinetic data which is required for reactor sizing

44 and better control of the overall process to yield a higher amount of the desired bio-oil product.

45 Inevitably, most studies on HDO reaction kinetics are centered on bio-oil model compounds

46 since bio-oils contain up to 300 different compounds and side reactions such as cracking,

47 decarbonylation, decarboxylation, hydrogenation, and hydrocracking also occur.[6-8,34-36] The HDO

48 performance of different catalysts has been tested using bio-oil and model compounds.

49 Undoubtedly, noble metals which include palladium (Pd), platinum (Pt), ruthenium (Ru), and

50 rhodium (Rh) remain the most promising because they are active at mild temperature. Mild

51 temperature reduces the occurrence of catalyst deactivation, a persistent problem in HDO

52 processes. Past studies on model compounds HDO over noble metals confirmed Pd as a leading

53 candidate among the listed metals. Some of the model compounds that have been used to

54 investigate the kinetics of HDO reaction include guaiacol, levoglucosan, acetic acid, anisole,

55 vanillin etc. Interestingly, more than four studies conducted to identify compounds present in bio-

56 oil reported vanillin. Hence, vanillin is the model compound of interest in this study. The reaction

57 kinetics of this compound has been reported only for Ru and Pt based catalysts. For instance,

58 Mahfud et al.[37], Huang et al.[38] and Bussetto et al.[15] all used homogenous Ru-based catalysts while

59 Bindwal et al.[39] used heterogeneous Ru–based catalyst and Sulman et al.[40] used heterogeneous Pt–

60 based catalyst. Hence, information on the reaction kinetics of vanillin over Pd – based catalyst

61 renowned for excellent performance in past HDO studies on model compounds and bio-oil is

62 missing.[41,42] To fill the identified knowledge gap, this study evaluated the influence of reaction

63 temperature, hydrogen gas pressure, catalyst loading and initial concentration on HDO reaction of

64 vanillin over Pd supported on activated carbon (Pd/C) in a batch reactor and ethyl acetate as the

65 solvent. Additionally, the effect of competitive adsorption between the products and vanillin was

66 evaluated, this is missing in literature on vanillin HDO reaction. Finally, this work examined the

67 effect of acetic acid on vanillin conversion to mimic possible changes in real bio-oil environment.

68 Notably external and internal mass transfer resistances were appropriately evaluated to ensure data

69 collection in the kinetically controlled regime. Langmuir- Hinshelwood-Hougen-Watson (LHHW)

70 models derived for competitive (Model I) and non- competitive (Model II) dissociative H_2

71 adsorption were fitted to the experimental data. The best fitted model was used to calculate the

72 reaction activation energy, enthalpy of adsorption for hydrogen and vanillin.

73

74 **2. EXPERIMENTAL SECTION**

75 **2.1. Materials.** Vanillin (purity 99%), Vanillyl Alcohol (4-hydroxy-3-methoxybenzyl alcohol,

76 purity 99%), Creosol (2-methoxy-4-methylphenol, purity 99%), Guaiacol (2-methoxyphenol,

77 purity 99%) and Ethyl Acetate (purity 99%) were all acquired through Sigma – Aldrich, United

78 Kingdom. Hydrogen (H_2) and Nitrogen (N_2) gas cylinders (purity 99.9%) were purchased from

79 BOC, United Kingdom. Commercial 10wt% Pd/C (Johnson - Matthey PLC Catalyst, United

80 Kingdom) was used. Micromeritics Analytical Instrument ASAP $^®$ 2010 was used determine the

81 catalyst surface area and pore volume according to ASTM C1274. The X-ray diffraction (XRD)

82 pattern was collected using Bruker AXS GmbH (D8 Advanced XRD, Karlsruhe, Germany). The

83 dispersion of Pd metal on the carbon support was determined using carbon dioxide chemisorption

84 with Quantachrome ChemBet Pulsar. The surface morphology of the catalyst before and after

85 reaction was examined via HITACHI TM3030 Plus Tabletop Scanning Electron Microscope

86 (SEM).

87   **2.2. Experimental Set – Up.** The experiments were carried out in a 100mL stainless steel

88   batch autoclave Parr instrument series (T_{max} = 648K, P_{max} = 10MPa) equipped with a mechanical

89   agitator and electric heating jacket to keep a constant reaction temperature. Figure 1 shows

90   schematic of the apparatus used to conduct the experiments. A pressure gauge with uncertainty of

91   ± 0.1MPa was used to monitor the pressure within the autoclave and a thermocouple with

92   uncertainty of ± 2K was used to measure the reaction temperature. Parr 4848 controller was used

93   to control the reaction temperature and speed of agitation throughout the experiments.

94   **2.3. Experimental Procedure.** In each experiment, a fixed amount of fresh 10% Pd/C catalyst

95   and $0.075dm^3$ solution containing the appropriate mass of vanillin (i.e. 0.40g - 0.74g) was charged

96   into the autoclave. N_2 gas was then used to purge the autoclave three times to create an inert

97   atmosphere for the intended reaction. With the agitator speed set at 150rpm, the autoclave content

98   was subsequently heated to the desired reaction temperature. At the desired reaction temperature,

99   the autoclave was pressurised by introducing H_2 gas and the agitator speed increased to 1000rpm.

100   The start time of each reaction was marked as the point of introducing H_2 gas into the autoclave.

101   Samples were collected in equally spaced time interval of 5mins during each reaction, the volume

102   of each sample was fixed at $0.0005dm^3$ to minimize pressure losses. Furthermore, H_2 gas was

103   added into the autoclave after each sample collection to maintain constant reaction pressure. This

104   procedure is the same as method described in the work of Bindwal et al.[43]
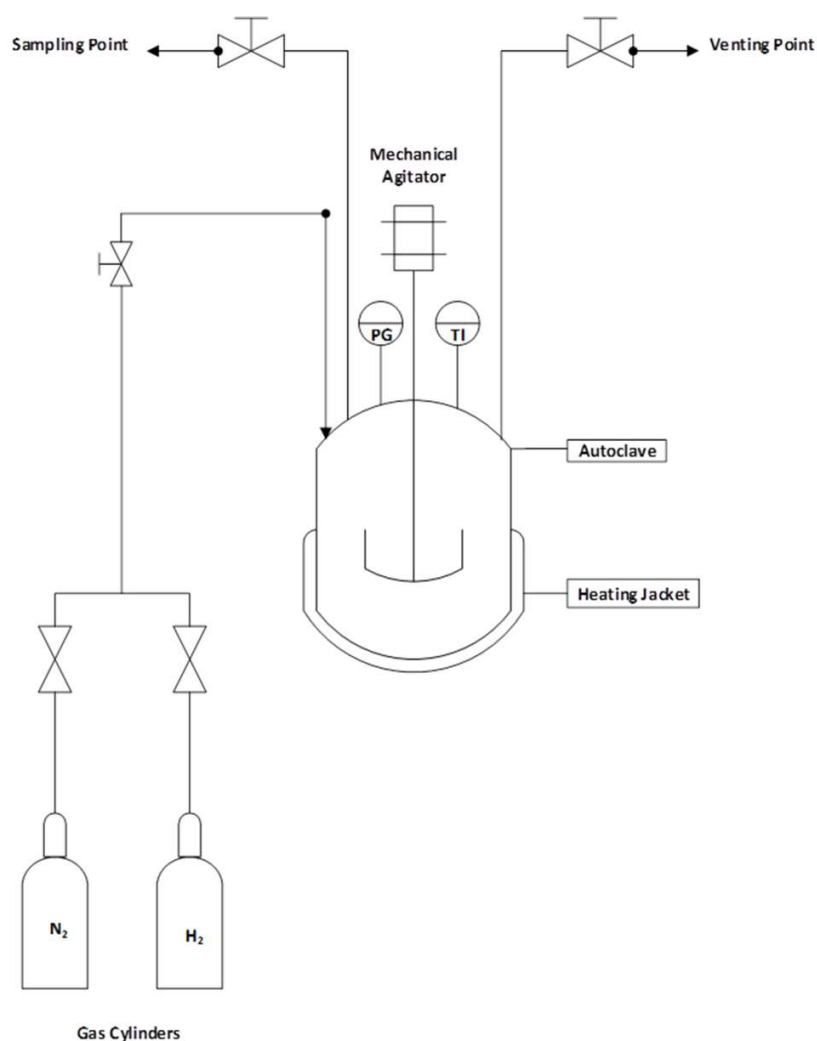
Figure 1. Schematic of Apparatus Set-up

The Antoine equation was used to compute the partial pressure of the solvent at each of the conditions investigated to establish H_2 gas partial pressures. The change in volume of the autoclave content and catalyst concentration was deemed negligible during each reaction. At the end of each reaction, the autoclave was cooled rapidly via an ice bath. Reproducibility of the experimental measurements was found satisfactory as they all lie within 10% standard deviation.

2.4. Product Analysis. Identification of the products present in the reaction samples was carried out through a gas chromatography unit equipped with mass spectrometry (GC-MS). In the

114   aftermath, a five point external calibration was used to quantify the amount of vanillin and products

115   within each of the liquid samples collected from reactions. To aid quantification, an automated

116   trace gas chromatography equipped with flame ionization detector (GC- FID) and mild polar

117   capillary column in the form of ZB-wax (specification: 250μm internal diameter, film thickness

118   of 0.25μm and 30m column length) was deemed suitable and used. The heating program applied

119   to analyse reaction samples via GC-FID include: a ramp from an initial oven temperature of 313K

120   at a rate of 283K/min to a final temperature of 523K which was then maintained for an additional

121   5minutes. A split ratio of 1:50 was used while the injector and detector temperature were held at

122   513K and 523K respectively.

123   **2.5. Mass Transfer Consideration.** HDO reaction of vanillin is an example of heterogeneous

124   reaction involving three phases, this includes: i) H_2 gas transfer from bulk gas phase to the gas –

125   liquid interface; ii) diffusion of H_2 gas through the gas – liquid interface into the bulk liquid; iii)

126   movement of H_2 gas to external surface of the catalyst particle ; iv) transfer of vanillin (VL) in

127   liquid phase to the external surface of the catalyst particle; v) intraparticle diffusion of VL and H_2

128   gas through the pores of the catalyst particles to the active sites for chemical reaction; vi) Diffusion

129   of the products out of the catalyst particles pore to the surface. Hence, the overall rate of vanillin

130   HDO reaction could be affected significantly by any of the listed steps. However, to achieve the

131   main objective of this work it is necessary to conduct all reactions in the kinetically controlled

132   regime. In this regime, reaction rates are independent of agitation speed and catalyst particle size

133   and thus allow accurate collection of kinetic data.[44] This effect was examined experimentally by

134   varying the agitation speed between 300 and 1100rpm; and by varying the catalyst particle size

135   between 80 and 260 μm. Further verification of any intraparticle mass transfer resistance was

136 carried out via the observable modulus ($\eta\phi^2$) using the Weisz and Prater criterion.[45] The following

137 equation was used to estimate the observable modulus ($\eta\phi^2$):

138 $$\eta\varphi^2 = \frac{r_0\omega L^2}{C_i D_{e_i}} \ , \quad \text{where i = VL, H}_2 \tag{1}$$

139 Herein, r_0 represents the initial reaction rate, η effectiveness factor, ϕ Thiele Modulus , ω catalyst

140 loading and L characteristic length of the spherical catalyst particle (L = d_p/6, where d_p = 90μm).

141 The correlation suggested by Pintar et al.[46] was used to estimate C_H (kmol/m^3) while Wilke –Chang

142 equation[47] was used to estimate the liquid phase effective diffusivities of VL and H_2.

3. RESULTS AND DISCUSSION

3.1. Catalyst Characterisation. The specific surface area of the 10%Pd/C catalyst obtained

145 using Brunauer-Emmett-Teller (BET) equation is 816.4 m^2.g^{-1}, pore volume 0.32 cm^3.g^{-1} and

146 average pore diameter 4.4 nm. The dispersion of Pd on surface of the C support is 28.1%. One of

147 the major challenges facing HDO commercialisation is catalyst deactivation due to deposition of

148 substances such as carbon, sulphur etc. on the catalyst surface.[48,49] Based on the micrographs

149 shown in Figure S1, no remarkable difference exists between the catalyst surface morphology

150 before and after the reaction. Thus, suggesting little or no significant deposition on the catalyst

151 surface as a result of the reaction that took place. This observation is consistent with claim in

152 literature that deactivation as a result of carbon deposition is less likely at low operating

153 temperatures.[33,49] The XRD pattern for raw and used Pd/C in Figure 2 further indicates that the

154 reaction did not induce significant changes. However, characteristic peak of palladium oxide

155 (PdO) around 002 plane at 2Θ = 35º in the raw Pd/C disappeared in the used Pd/C XRD pattern.

156 A plausible reason for this disappearance is that PdO reduces to metallic palladium (Pd) in the

157 hydrogen reaction environment. Hence, intensity of the diffraction peak around 111 plane

158 attributed to Pd at 2Θ = 40º increased in the used Pd/C XRD pattern. Additionally, the broad peak

159 around $2\Theta = 25°$ corresponds to carbon while the remaining peaks at 47° (200), 68° (220) and 82°

160 (311) are attributed to Pd (200), Pd (220) and Pd (311). To reaffirm the claim of negligible

161 deposition and deactivation, findings from investigation into reusability of the catalyst are reported

162 in section 3.10.

163

164
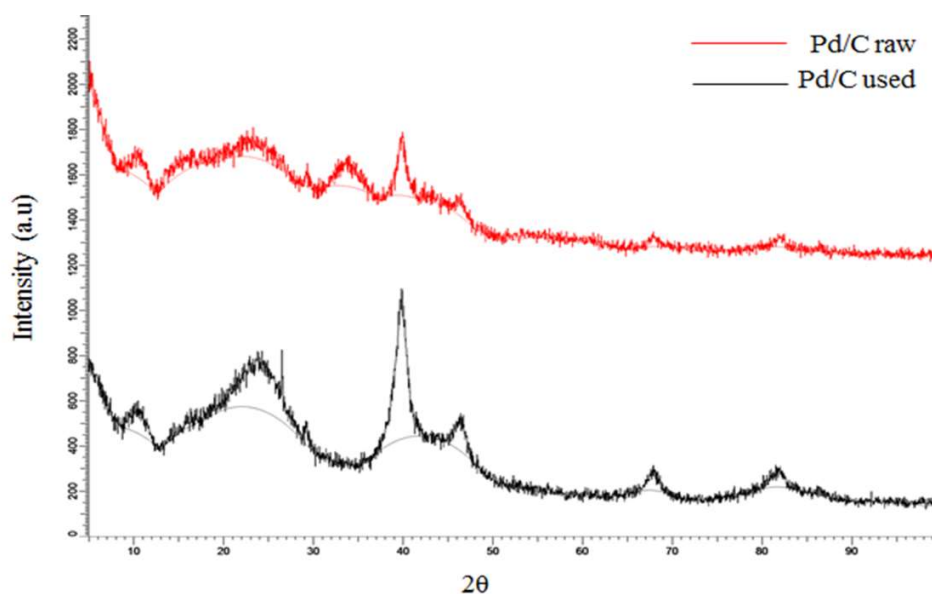
165 **Figure 2. XRD pattern of the raw and used Pd/C catalyst.**

166

167 **3.2. External Mass Transfer verification.** The result of experiments conducted to examine

168 influence of agitation speed on conversion is represented in Figure 3. It shows that conversion

169 increased from 84% to 94% as agitation speed increases from 300rpm to 900rpm. However, further

170 increase in the agitation speed from 900 to 1100rpm showed no change in conversion. Hence,

171 subsequent experiments in this work were carried out using 1000rpm to prevent external mass

172 transfer interference.

9

173

Figure 3. Effect of agitation speed on VL conversion at T=338K, P_H = 1.0MPa, C_{VL0} = 65.0mM, t = 30mins and ω = 0.27kg/m³.

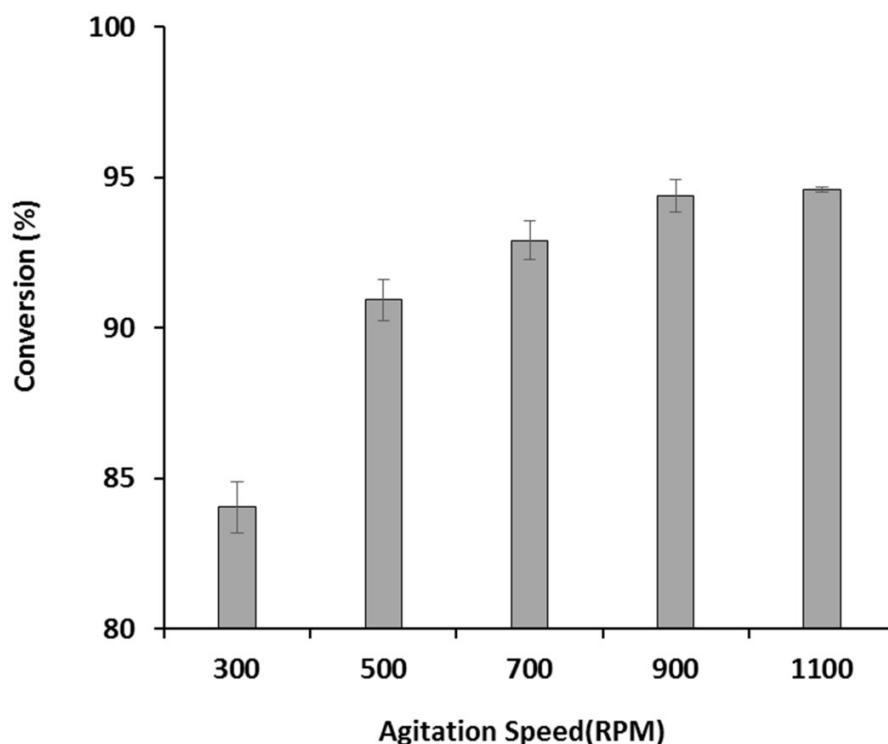Preliminary experiments were carried out at agitation speed 1000 rpm, temperature 338K, and hydrogen gas pressure 1.0 MPa with no catalyst, activated carbon (0.27 kg/m³) and 10%Pd/C (0.27 kg/m³) using 67mM initial vanillin (VL) solution. The results from these preliminary experiments are shown in Table 1. Without catalyst only about 2% conversion was achieved with negligible products formed, while the addition of activated carbon increased the conversion to 8% compared to 98.7% obtained when 10%Pd/C was used. The 6% additional increase with activated carbon over blank experiment suggest that activated carbon function as a hydrogen transfer mediator while the significant increase with 10%Pd/C implies Pd is largely responsible for VL HDO reaction.

184

185 **Table 1. Results from Blank, activated carbon and Pd/C VL HDO Reactions.**

Experiments	C_{VL}	C_{va}	C_{cr}	X (%)
No Catalyst	65.9	0.8	0.2	1.8
Activated Carbon (C)	61.7	3.3	2.2	8.0
Pd/C	0.88	58.9	12	98.7

186

187 **3.3. Internal Mass Transfer verification.** Figure 4 depicts the effect of particle size, it shows

188 that conversion increased from 33% to 57% as the particle size decreases from fraction over 250μm

189 to fraction less than 250μm but greater than 180 μm. But further decrease in size of the catalyst

190 particle below 180 μm did not induce significant changes in conversion. This result suggests

191 intraparticle mass transfer resistance is negligible for particles less than 250 μm. Hence, 90 μm

192 size catalyst particles were used in subsequent experiments.

193
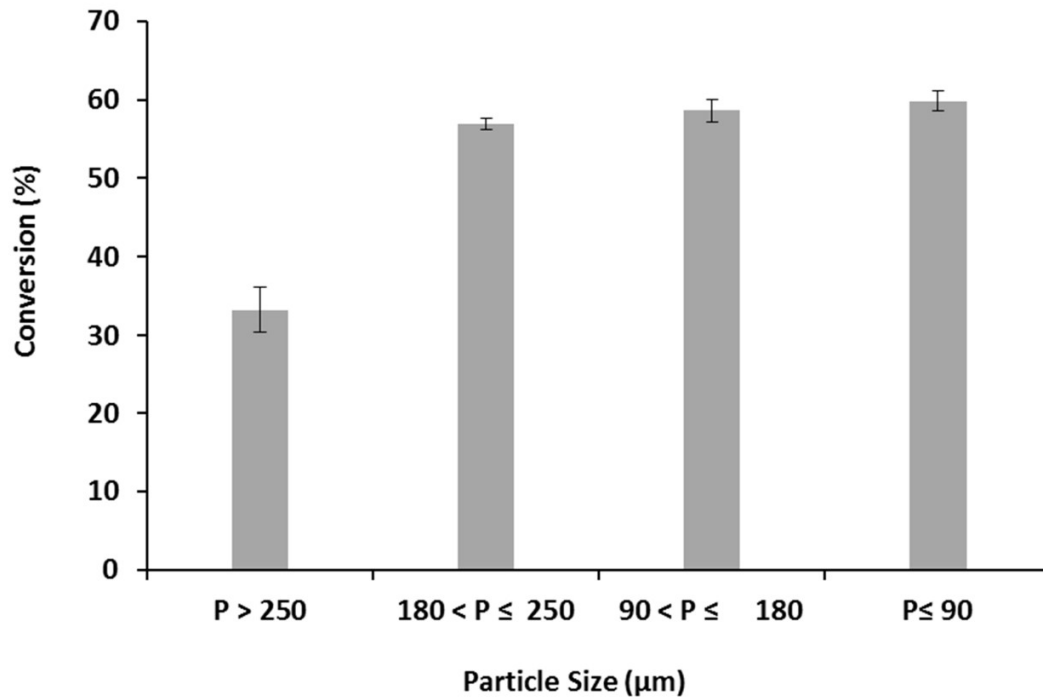
Figure 4. Effect of catalyst particle size on VL conversion at 1000rpm, T = 338K, P_H = 1.0MPa, C_{VL0} = 65.0mM, t = 30mins and ω = 0.27kg/m^3.

The results of numerical evaluation based on equation 1 to examine intraparticle mass transfer resistance are presented in Table 2. From the definition of observable modulus in equation 1, a value less than unity is desirable as it suggests quicker mass transfer rate than reaction rate, which implies a reaction - controlled system.

Table 2. Values of Observable Modulus at 338K

Parameter	Values		
ω (kg/m^3)	0.13	0.20	0.27
C_{VL0} (mM)	65.0	65.0	65.0
C_{H2} (mM)	1.2	1.2	3.6
$r \times 10^2$ (kmol/(kg$_{cat.}$ min))	2.06	1.72	2.01
L (m)	15×10^{-6}	15×10^{-6}	15×10^{-6}
$D_{e,VL} \times 10^9$ (m^2/s)	2.13	2.13	2.13
$D_{e,H2} \times 10^8$ (m^2/s)	1.89	1.89	1.89
$\eta\Phi_{vl}^2$	5.58×10^{-8}	9.31×10^{-8}	1.63×10^{-7}
$\eta\Phi_{H}^2$	3.41×10^{-7}	5.68×10^{-7}	3.32×10^{-7}

206

207   Indeed, for both reactants i.e. VL and H$_2$ gas, Table 2 shows that the observable modulus values

208   found were much less than unity. Thus, provides additional evidence that intraparticle mass

209   transfer resistance is negligible in the range of conditions considered. A typical concentration-time

210   profile observed in the course of studying VL HDO reaction is presented in Figure 5. It clearly

211   indicates the formation of vanillyl alcohol (VA) and creosol (CR) as products from the reaction

212   since their concentration increases over time as vanillin concentration decreases.
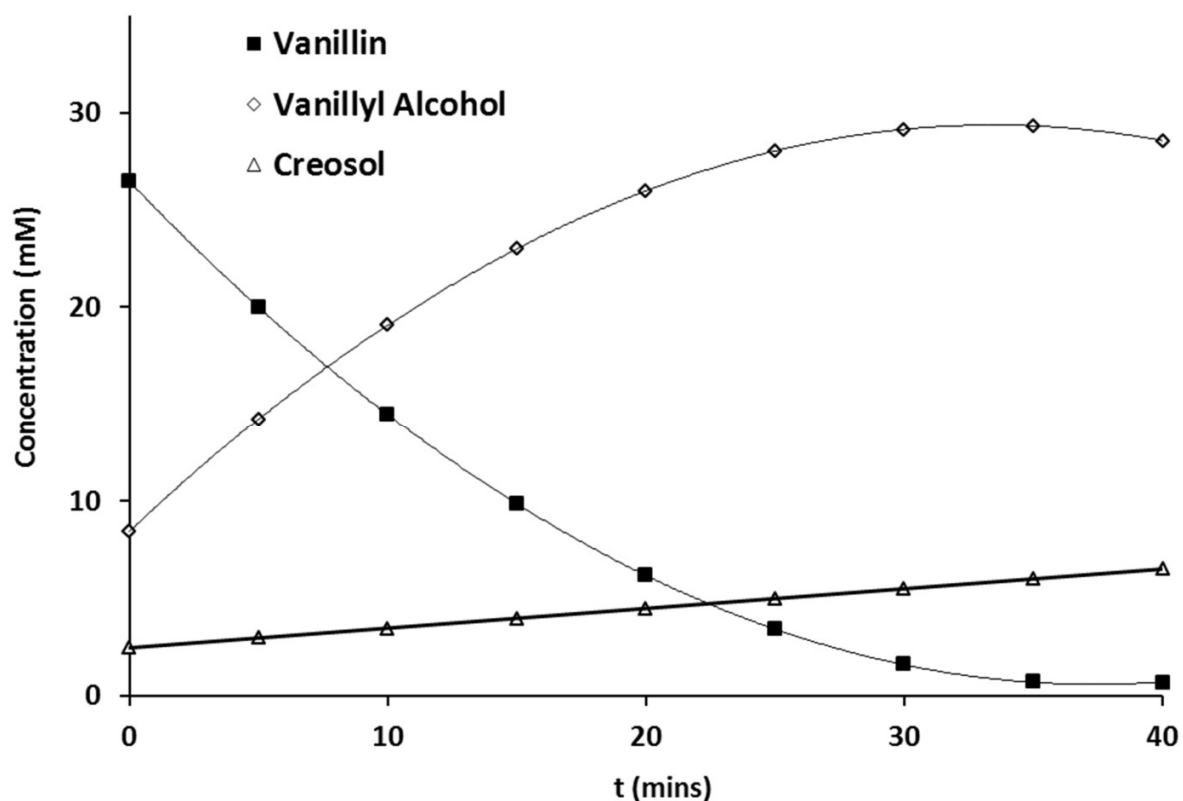
213

Figure 5. Typical concentration against time profile at 1000rpm, T = 338K, P_H = 1.0MPa, C_{VL0} = 35.0mM and ω = 0.13kg/m^3. Lines represent best polynomial fit to the data.

3.4. Effect of Catalyst Loading. The effect of changes in catalyst loading (ω) on initial rate of VL disappearance (r_0) was examined over the range of 0.13 to 0.27kg/m^3 at 318K, 328K and 338K, the values of hydrogen gas partial pressure (P_H) and initial vanillin concentration (C_{VL0}) used were 1.0MPa and 65.0mM respectively. Figure S2 represents the conversion-time and the corresponding rate-time plots due to changes in catalyst loading. The initial rates of VL disappearance were calculated by differentiating 2nd order polynomial fitted to the conversion-time data at various times over the course of each reaction and the rate-time line derived was extrapolated to the initial time (i.e. t=0). This method of determining initial reaction rate has been reported elsewhere,[50] Figure S2 illustrates how this method was applied to these data. Figure 6 summarises the changes

225 observed in initial rate of VL disappearance following changes to the catalyst loading, highlighting

226 a directly proportional change in initial VL disappearance rates with respect to catalyst loading.

227 This provides supplementary evidence that reactions examined are within the kinetically controlled

228 regime. However, since these lines do not pass through the origin, it must be concluded that the

229 reaction exhibits non-first order kinetics with respect to catalyst loading over the range of
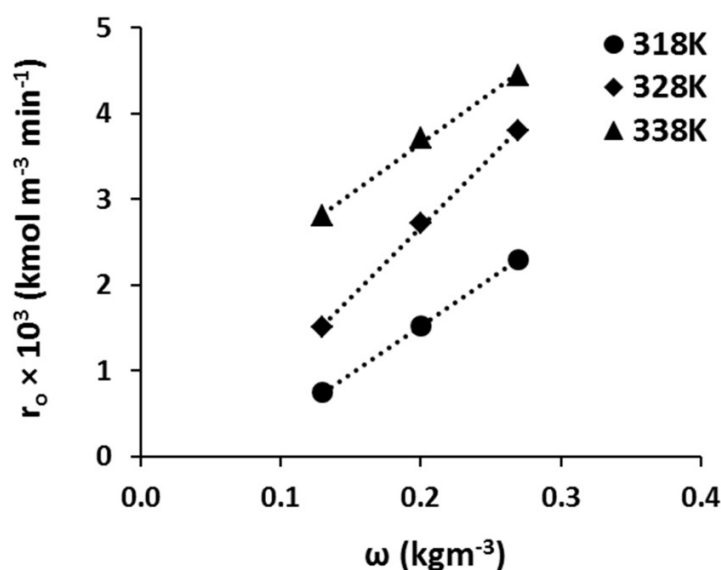
230 temperatures investigated.

231

Figure 6. Effect of catalyst loading on VL initial rate of disappearance at 1000rpm, $P_H = 1.0$MPa and $C_{VL0} = 65.0$mM. Lines represent best linear fit to the data.

234 **3.5. Effect of H_2 gas Partial Pressure.** The influence of hydrogen gas partial pressures (P_H) on

235 initial rates of VL disappearance (r_0) was investigated over the range of 1.0 to 3.0MPa at 318K,

236 328K and 338K with the values of initial VL concentration (C_{VL0}) and catalyst loading (ω) kept at

237 65.0mM and 0.27kg/m^3 respectively. Figure S3 shows the conversion-time and the corresponding

238 rate-time plots due to changes in P_H. Figure 7 depicts observed variation in the initial rates of VL

239 disappearance (r_0) following changes in hydrogen gas partial pressure (P_H) at the various

240 temperatures considered. At 318K, it can be seen that r_0 increased from 0.72×10^{-2} to 1.00×10^{-2}

241 kmol/kg$_{cat}$ min as P_H increases from 1.0 to 3.0MPa. Likewise at 338K, r_0 increased from 1.71×10^{-2}

242 to 2.01×10^{-2} kmol/kg$_{cat}$ min following changes in P_H from 1.0 to 3.0MPa. Hence, an increase in

243 H$_2$ gas partial pressure enhances the initial rate of VL disappearance. This observation can be

244 linked to the increase in amount of H$_2$ available for reaction as a result of increase in P_H.
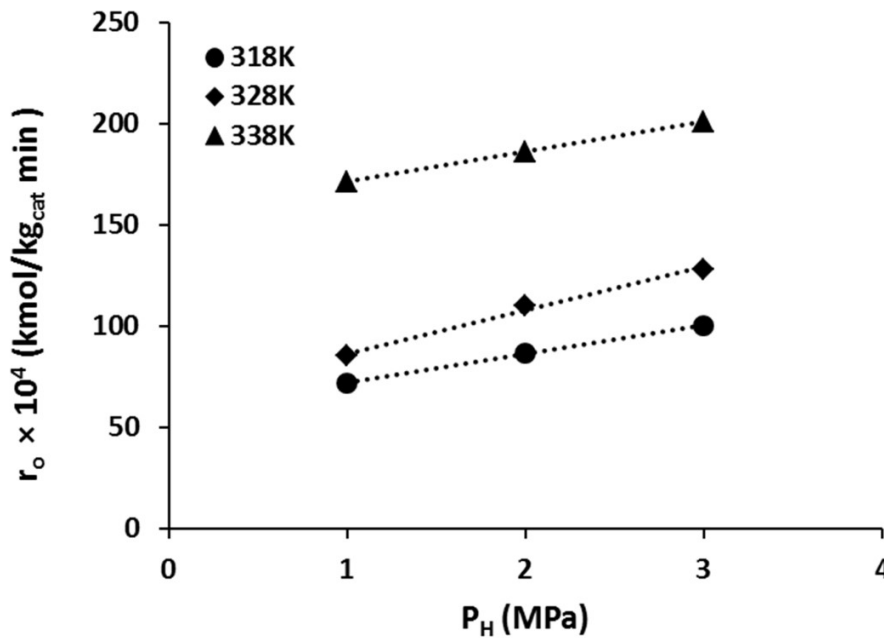

245

246 **Figure 7. Effect of H$_2$ gas partial pressure (P_H) on initial rates of VL disappearance at 1000rpm, C_{VL0}**

247 **= 65.0mM and ω = 0.27kg/m^3. Lines represent best linear fit to the data.**

248 From the plot of $In(r_0)$ against $In(P_H)$ shown in Figure S4, the slope corresponds to order of

249 reaction with respect to hydrogen gas pressure and the value lies between 0.14 and 0.30. This

250 thereby indicates that VL HDO reaction exhibits non-first order kinetics with respect to hydrogen

251 gas partial pressure.

252 **3.6. Effect of initial VL concentration.** The effect of initial VL concentration (C_{VL0}) on the

253 initial rate of VL disappearance (r_0) was investigated over the range of 35 to 65mM at 318K, 328K

254 and 338K with the values of P_H and ω kept at 1.0MPa and 0.13kg/m^3 respectively. Figure S5 shows

255 the conversion-time and the corresponding rate-time plots due to changes in C_{VL0}. Figure 8 shows

256 observed changes in r_0 as C_{VL0} increases from 35mM to 65mM at different reaction temperatures.

257 It can be seen that r_0 decreased from 3.04×10^{-2} to 2.16×10^{-2} kmol/kg$_{cat}$min as C_{VL0} increases

258 from 35mM to 65mM at 338K. Similar observation of r_0 decreasing as C_{VL0} increases from 35mM

259 to 65mM can be seen at 318K and 328K. This observation is contrary to normal expectation of

260 rate increasing with concentration; however, this indicates decreased catalytic activity as C_{VL0}

261 increases. A plausible reason for the observed trend in activity is that competition among the

262 reactants for finite number of sites on the catalyst increases as C_{VL0} goes up. Modelling of the

263 reaction kinetics in Section 3.11 will help shed light on this interesting but unusual trend. In the

264 study of 1-heptyne hydrogenation over alumina supported Pd and Ni catalysts by Maccarrone et

265 al.,[41] activity of both catalysts decreased as the starting concentration of 1-heptyne increased.

266 Therefore, indicates that the observed phenomenon of initial reaction rate decreasing with increase

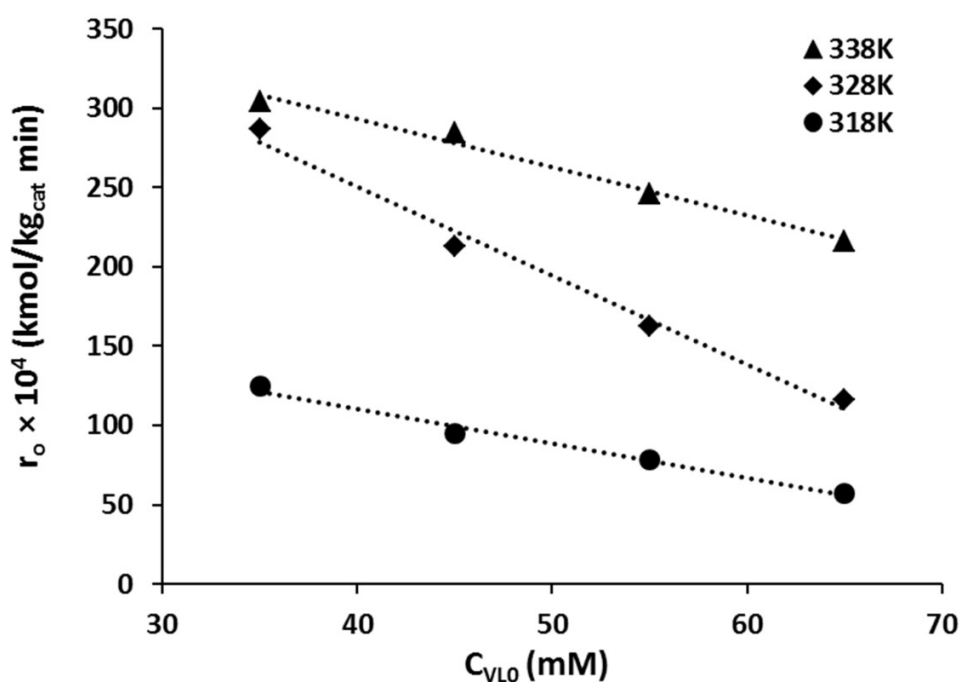267 in the starting reactant concentration is unusual but possible in heterogeneous catalysed reaction.

268

Figure 8: Effect of initial VL concentration on initial rate of VL disappearance at 1000rpm, P_H =1.0MPa and ω = 0.13kg/m³. Lines represent best linear fit to the data.

Interestingly, the effect of changes in catalyst activity following increase in C_{VL0} was most noticeable at 328K with the initial rate of VL disappearance declining by approximately 5×10^{-4} kmol/kg$_{cat}$ min for every mM increase in the starting VL concentration. Figure S6 depicts the linearised relationship derived from plotting $\ln(r_0)$ against $\ln(C_{VL0})$, while the gradients of the lines obtained confirm an order of reaction with respect to vanillin concentration between -0.7 and -1.2. This indicates a non-first order dependence on concentration, suggesting a Langmuir-Hinshelwood (L-H) type of rate expression may be suitable in describing VL HDO reaction kinetics.[50] The unusual trend in activity of the catalyst as C_{VL0} increases, further indicate that the development of kinetic model for VL HDO reaction in Section 3.11 requires consideration of processes such as adsorption, surface reaction and desorption occurring on the catalyst surface.

3.7. Effect of Temperature. It is a well-known fact that reaction rate tends to generally increase with temperature. The trends in the VL HDO reaction presented so far confirms this notion. Table 3 summarises changes in product distribution and conversion with respect to the reaction temperature. In general, selectivity to the deoxygenated product creosol (S_{CR}) increased as the reaction temperature increases. Conversely, selectivity to vanillyl alcohol (S_{va}), the intermediate product, reduced as reaction temperature increases. Interestingly, Bindwal et al.[39] reported similar observations of changes in product distribution following changes in reaction temperature.

Table 3. Product Distribution as a Function of Initial VL Concentration and Temperature (ω = 0.13kg/m³, P_H = 1.0MPa).

C_{VL0} (mM)	T(K)	X (%)	S_{va} (%)	S_{CR} (%)

	318	74.0	87.4	12.6
35	328	96.0	81.0	19.0
	338	97.0	80.8	19.2
	318	62.0	88.4	11.6
45	328	91.0	86.4	13.6
	338	96.0	84.6	15.4
	318	52.0	86.6	13.4
55	328	76.0	88.9	14.1
	338	84.0	85.3	14.7
	318	46.0	91.2	8.8
65	328	72.0	87.8	12.2
	338	82.0	87.4	12.6

291

292   The equivalent turnover frequencies (TOF) from this study ranges from 2.2 to 12 min^{-1}, these

293 are lower than values reported in similar work by Bindwal et al.[39] using 5% Ru/C (metal dispersion

294 2.74%). Hence, the observed discrepancies in TOF can be attributed to the significant difference

295 in metal loadings and dispersion on carbon support.

296

297   **3.8. Effect of the reaction products on conversion.** To examine the effect of products on

298 conversion, 0.12-0.64g of VA and 0.10-0.52g of CR were added to the initial VL solution and used

299 to conduct VL HDO reaction. Figures 9 and 10 summarises findings from the investigation. It can

300 be seen from Figure 9 that the presence of VA in the starting reaction mixture improves the rate at

301 which VL changes, with 99.6% and 88.2% of initial VL converted after 40 minutes when the

302 starting mixture contained 10mM VA and 55mM VA, respectively. In the absence of VA under

303 the same condition, 76% conversion was achieved in 40 minutes. This result shows that the

304   presence of VA in the reaction mixture promotes conversion of VL. However, the promoting effect

305   diminished as initial concentration of VA increases from 10mM to 55mM. This suggests an

306   increased competition between VL and VA for a finite number of sites on the catalyst surface.
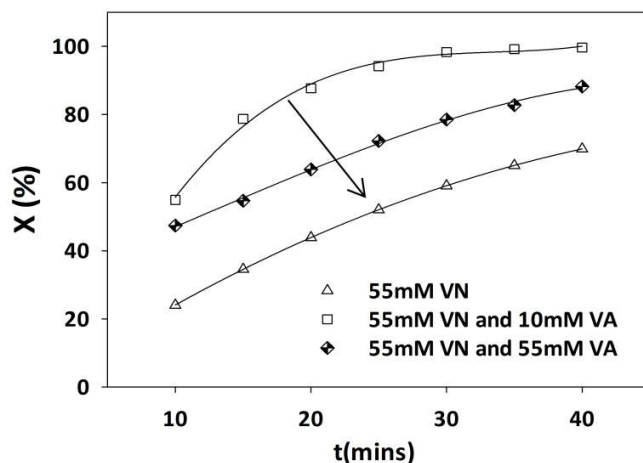
307

308

309   **Figure 9. Effect of VA on conversion at 1000rpm, T=328K, P_H = 1.0MPa and ω = 0.13kg/m³. Lines**

310   **represent best polynomial fit to the data.**

311   Figure 10 shows that the presence of CR in the starting mixture enhances conversion. Conversions

312   of 98.8% and 96.5% were achieved after 40 minutes reaction when the starting mixture contained

313   10mM CR and 55mM CR, respectively. However, an increase in concentration of CR in the

314   starting mixture from 10 to 55mM clearly had less effect on conversion than addition of the initial

315   10mM. Based on this analysis of the influence of reaction products on conversion, it seems the

316   competition between VL and VA for sites on the catalyst surface is stronger than competition

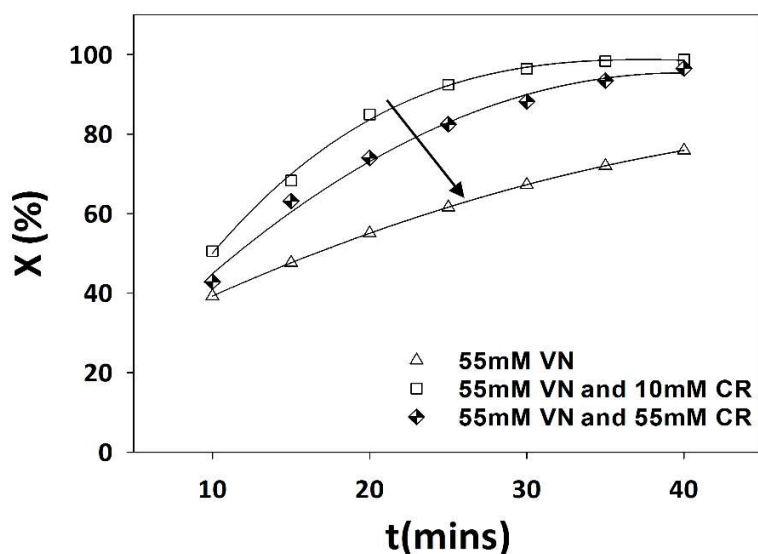317   between VL and CR. It is clear that both products induced an autocatalytic effect (Figures 9 and

318   10).

319

Figure 10. Effect of CR on conversion at 1000rpm, T = 328K, P_H = 1.0MPa and ω = 0.13kg/m³. Lines

represent best polynomial fit to the data.

3.9. Effect of Acetic acid on conversion. Since acetic acid is one of the major components

within bio-oil, VL HDO reaction in the presence of known acetic acid concentration was carried

out. The concentration ratios of VL and acetic acid selected for this purpose reflects the ratio in

which the two models commonly exist in a typical bio-oil.[16] Figure 11 represents the effect of

acetic acid on conversion, it clearly shows that conversion increased from 88.9% (no acetic acid)

to 100% (in the presence of acetic acid) after 60 minutes of reaction. A noticeable difference was

also observed in the distribution of products formed after 60 minutes reaction, with the selectivity

to CR increasing from 8.3% (no acetic acid) to 22.8% (in the presence of acetic acid) and

selectivity to VA decreasing from 91.7% (no acetic acid) to 77.2% (in the presence of acetic acid).

The observed trend in conversion and product distribution indicates improved rate of VL

transformation to VA and VA transformation to CR. This consequently suggests that hydrogen

molecules are more readily available to react with both unreacted VL and VA when VL HDO

334   reaction occurs in the presence of acetic acid. This observation is in agreement with findings from
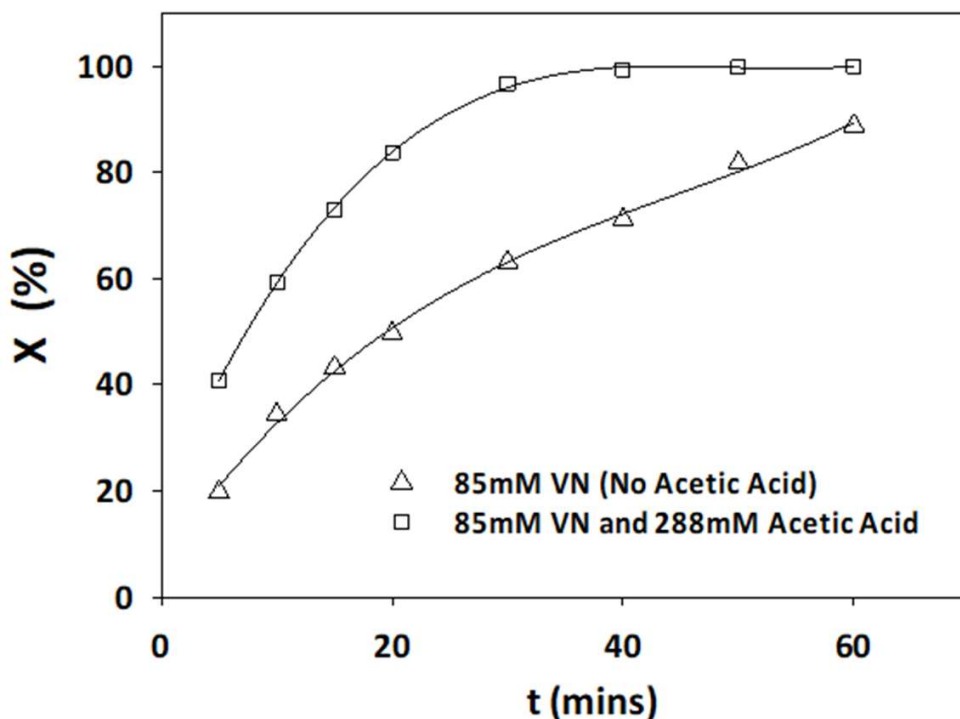
335   the work of Huang et al.[38]

336

Figure 11. Effect of acetic acid on conversion rates at 1000rpm, T = 318K, P_H = 1.0MPa and ω = 0.27kg/m³ . Lines represent best polynomial fit to the data.

339   **3.10. Catalyst Reusability Test.** The reusability of Pd/C catalyst was investigated over three

340   consecutive reaction runs at 338K with an initial VL concentration of 263mM, hydrogen gas partial

341   pressure of 2.0MPa, catalyst loading of 6.7kg/m³ and reaction time of 1hr. The catalyst recovered

342   from each run was dried overnight at room temperature before reuse. Figure 12 depicts changes in

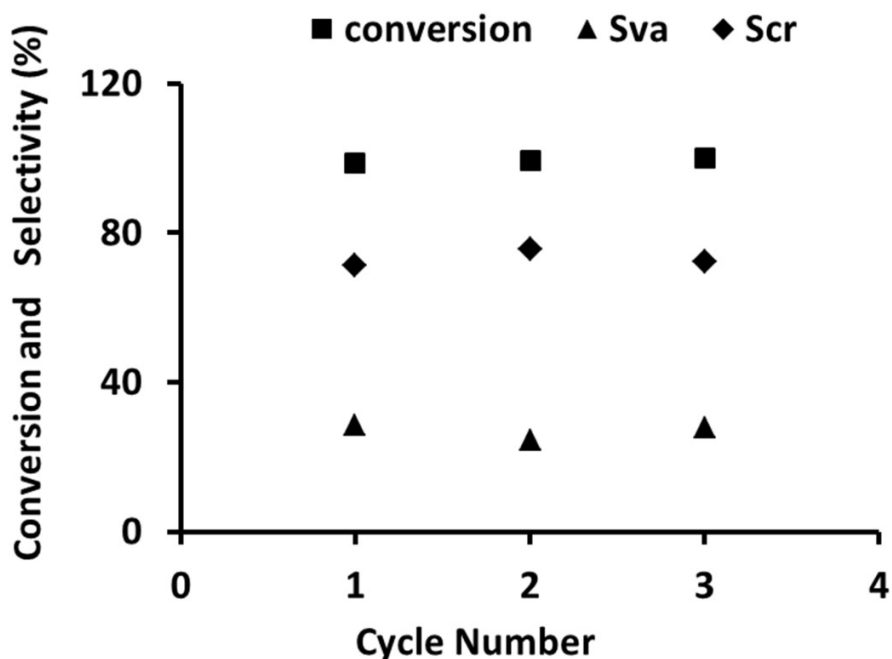343   conversion and distribution of products after each run.

344

345

Figure 12. Effect of catalyst reuse on Conversion and Product distribution at 1000rpm, T = 338K, P_H = 2.0MPa, C_{VL0} = 263mM, t = 1hr and ω = 6.7kg/m^3.

It is clear from Figure 12 that the conversion and distribution of products did not change considerably between successive runs. This reinforces previous suggestion of negligible catalyst deactivation in Section 3.1. Hence, the kinetic model describing VL HDO reaction does not require a deactivation term. Proposed sequence for VL HDO over Pd/C catalyst is shown in reaction scheme 1. The first step involves hydrogenation of VL to form the intermediate product Vanillyl Alcohol (VA), further hydrogenation transforms VA to the deoxygenated product creosol (CR). Notably this sequence is in agreement with thermodynamics, since the methoxy (-OCH$_3$) group on VL requires higher energy input to dissociate compared to the carbonyl (- CHO) group. The required energy for methoxy group dissociation is not achievable at the mild conditions used in this work, thereby accounts for the two products VA and CR detected. Under harsh conditions

358 involving temperature above 338K, unexpected products from side reactions such as

359 demethylation may appear.

360

361
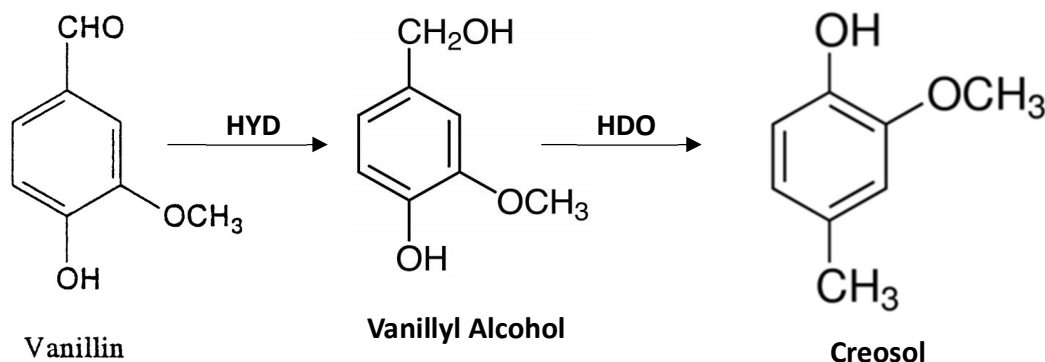
367 **Reaction scheme 1. The HDO reaction steps for vanillin.**

368

369 **3.11. Mechanism of the Reaction and Kinetic Modeling.** In most studies on fluid solid catalytic

370 reactions, rate equations are derived through dual site Langmuir-Hinshelwood-Hougen-Watson

371 (LHHW) approach. The benefits of this approach are: i) it takes into account all processes

372 occurring on the surface of the Pd/C catalyst such as adsorption, desorption and surface reaction,

373 and ii) derived rate equations can be extrapolated to concentrations outside the experimentally

374 measured values. The alternative approach of establishing ordinary differential equation (ODE)

375 from mass balances on reactants and products does not offer the listed benefits of LHHW approach.

376 Besides, ODE approach often requires assumption of first-order reaction for both reactants and

377 products; this is not the case with the kinetic data collected so far. Hence, two plausible rate

378 equations derived from the dual site LHHW approach under the assumption of dissociative

379 chemisorbed hydrogen are presented in Table 4 (see derivation in supplementary information

380 Section S1). These rate equations have been reported previously in the work of Bindwal et al. on

381   VL hydrogenation.[39] However, they were simplified into an overall second order expression in the

382   work of Bindwal et al.[39] In this study, suitability of the derived rate equations in Table 4 to the

383   experimental data is examined. The series of elementary steps that governs model I describing

384   competitive adsorption of dissociatively chemisorbed H_2 and VL are represented by equations 2

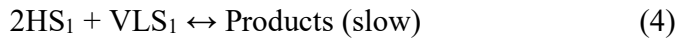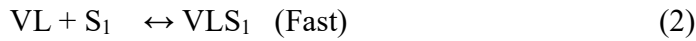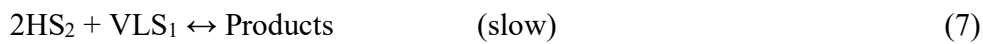385   to 4 (see derivation in supplementary information Section S1).

386     $VL + S_1 \leftrightarrow VLS_1$ (Fast)   (2)

387     $H_2 + 2S_1 \leftrightarrow 2HS_1$ (Fast)   (3)

388     $2HS_1 + VLS_1 \leftrightarrow$ Products (slow)   (4)

389

390   **Table 4. Rate Expressions for Plausible Kinetic Models**

Model	Rate Expression	Model Description
I	$r = \dfrac{k_s K_H K_{VL} C_H C_{VL}}{\left(1 + \sqrt{K_H C_H} + K_{VL} C_{VL}\right)^3}$	Competitive adsorption of dissociative H_2 and VL
II	$r = \dfrac{k_s K_H K_{VL} C_H C_{VL}}{\left(1 + \sqrt{K_H C_H}\right)^2 (1 + K_{VL} C_{VL})}$	Non – Competitive adsorption of dissociative H_2 and VL

391

392   While for Model II describing non-competitive adsorption of dissociatively chemisorbed H_2 and

393   VL, the associated elementary reactions are represented by equations 5 to 7 (see derivation in

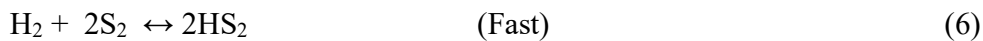394   supplementary information Section S1).

395     $VL + S_1 \leftrightarrow VLS_1$ (Fast)   (5)

396     $H_2 + 2S_2 \leftrightarrow 2HS_2$ (Fast)   (6)

397     $2HS_2 + VLS_1 \leftrightarrow$ Products   (slow)   (7)

398
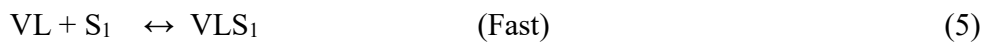
399   The other plausible rate expressions with either vanillin or hydrogen adsorption as the rate

400   determining steps for competitive and non-competitive dissociative chemisorption derivations are

401   presented in Section S1.

402   The linearised format of rate equations presented in Table 4 was used to assess the fit of models

403   I and II to the experimental data. At constant hydrogen gas partial pressure (P_H) of 1.0MPa, plots

404   of C_{VL0} vs $(C_{VL0} / r_0)^{1/3}$ should be linear for model I, while for model II the plot of C_{VL0} vs $(C_{VL0} / $

405     $r_0)$ should be linear. A coefficient of determination (R^2) with value greater than or equal to 0.99

406   indicates a good fit to the experimental data. Clearly from Figures 13a and 13b, model I with R^2

407   values between 0.995 and 0.998 predicts the experimental data better than model II with R^2 values

408   between 0.959 and 0.989. For this reason, model I is deemed the most suitable fit and model II is

409   discarded. This analysis complement initial finding of competitive adsorption mentioned in section
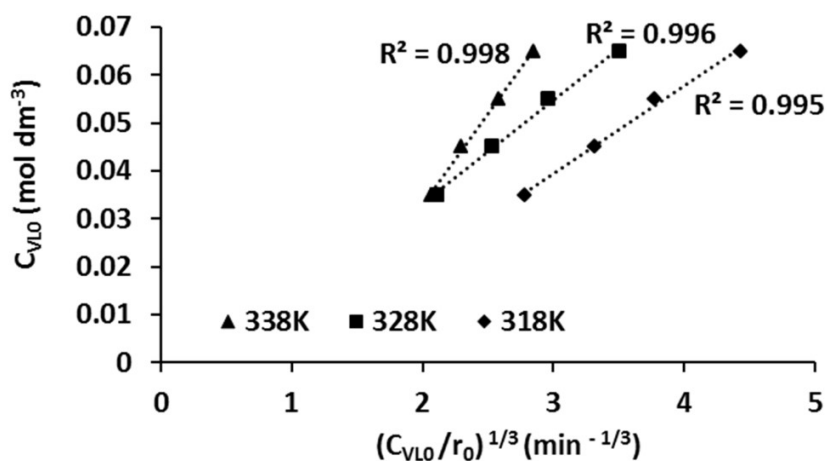
410   3.6.

411

412 **Figure 13a. Fit of Linearised Version of Model I to Experimental data. Lines represent best fit to the**
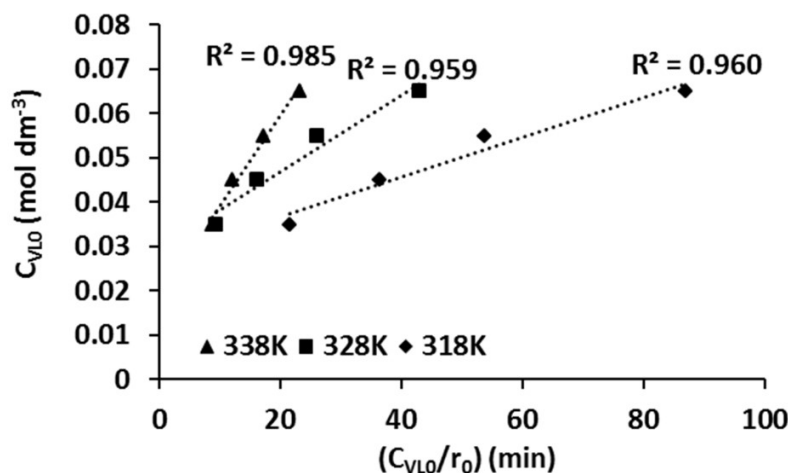
413 **data.**

414

415 **Figure 13b. Fit of Linearised version of Model II to Experimental Data. Lines represent best fit to**

416 **the data.**

417 Non-competitive adsorption with either vanillin or hydrogen adsorption as the rate determining

418 step reduces to first order equations (see eq.61 and eq.72 in Section S1). However, as shown in

419 Figure S7, the fit of competitive adsorption model with hydrogen chemisorption as the rate

420 determining step to the experimental data is less than 99% (eq. 39).

421 A non-linear generalized reduced gradient (GRG) solver on Microsoft Excel was used to

422 estimate kinetic parameters which include surface reaction rate constant (k_s), hydrogen equilibrium

423 constant (K_H) and VL equilibrium constant (K_{VL}) using model I. The objective function minimized

424 to solve the model was residual sum of squares (RSS) defined in equation 8.

425 $$RSS = \sum (r_{exp} - r_{mod})^2 \qquad (8)$$

426 where r_{exp} and r_{mod} represents the experimental reaction rates and reaction rates computed from

427 the models respectively. Table 5 summarises the estimated values for the reaction rate constant,

428 activation energy, enthalpy of adsorption for hydrogen and vanillin.

429

Table 5. Estimated rate constant, adsorption constants, heat of adsorption and activation energy

Model	T (K)	K_s (kmol/kg$_{cat}$ min)	K_H (m^3/kmol)	K_{VL} (m^3/kmol)	E_A (kJ/mol)	ΔH_H (kJ/mol)	ΔH_{VL} (kJ/mol)
I	318	12.29 ± 0.10	10.25 ± 0.13	14.41 ± 0.03	50.61	28.89	32.46
	328	25.02 ± 1.91	8.80 ± 0.81	11.21 ± 0.07			
	338	38.06 ± 0.03	5.35 ± 0.01	6.95 ± 0.20			

The Arrhenius expression was used to estimate the reaction activation energy, while Van't Hoff isochore was used to estimate the enthalpy of adsorption. Figure 14 represents the parity plot for model I, indicating strong agreement between the experimental reaction rates and predicted reaction rates with an R^2 value greater than 99% to support this claim. In addition, Figure 15 shows that the predicted VL concentration from model I matches the experimental VL concentration at different point of the reaction at T=318K, 328K and 338K. This provides further confirmation that model I accurately describe the kinetics of VL HDO reaction conducted in a batch reactor.
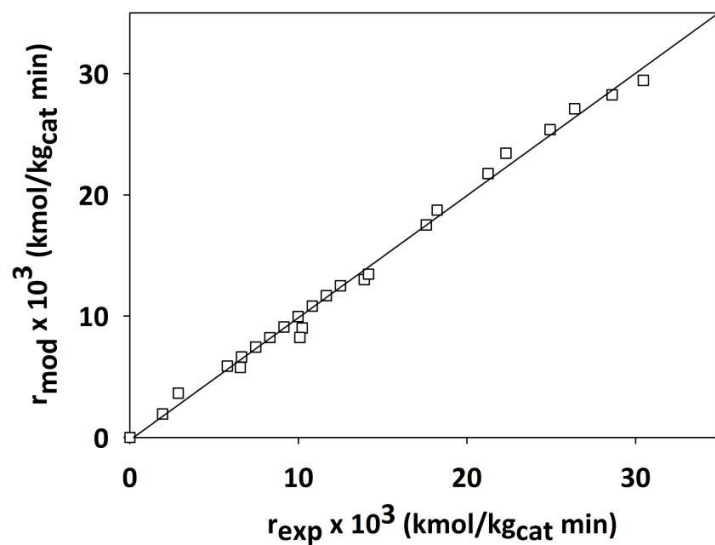
Figure 14. Parity Plot of model I to compare predicted reaction rates and experimental reaction rates. Lines represent best fit to data.

The estimated activation energy of 50.6kJ/mol is significantly greater than typical activation energy in mass transfer limited system (12 - 21kJ/mol), thus indicating that experimental data were collected in the kinetically controlled regime.[37,51-53]. This reinforces the conclusion of negligible external and internal mass transfer effect in Sections 3.2 and 3.3.

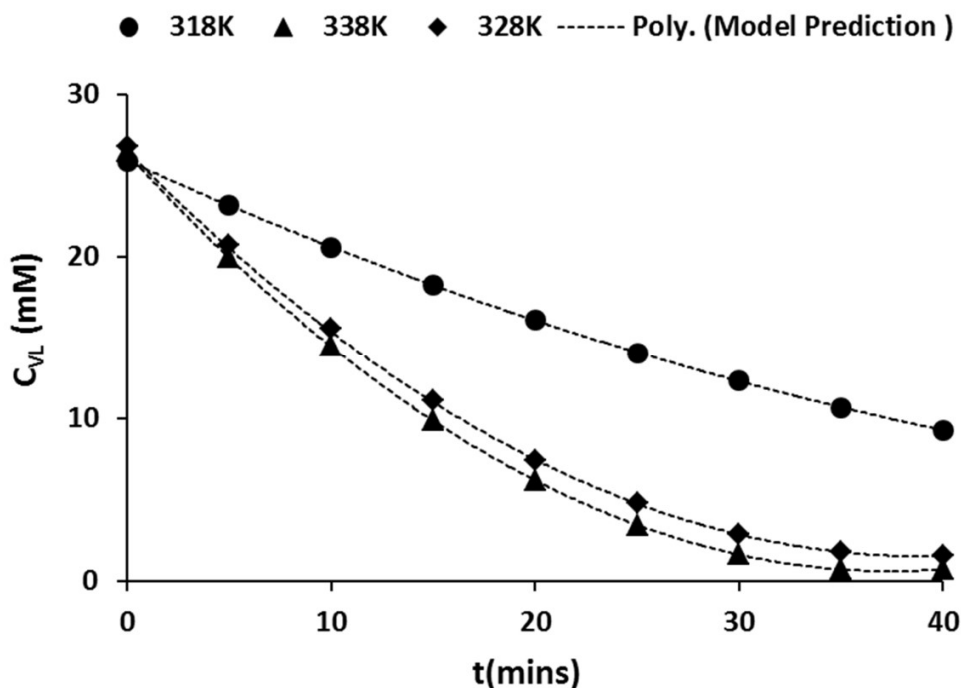**Figure 15. Comparison of changes in predicted concentration of vanillin and experimental values at 318, 328 and 338K (P_H = 1.0MPa, $C_{VL, 0}$ = 35.0mM and ω = 0.13kg/m^3). Lines represent fit of model to experimental data.**

In comparison to a value of 41.2kJ/mol reported in the work of Bindwal et al.[40] as activation energy for VL hydrogenation, it is clear that the estimated value for VL HDO reaction activation energy from this work is within the same order of magnitude. Of course, the little difference could be attributed to simplifications of LHHW models to an overall second order reaction in Bindwal et al.[40] and other factors such as difference in solvent and active element. Looking at magnitude of the estimated enthalpy of adsorptions for VL and H$_2$ in Table 5, it can be concluded that both reactants adsorbed weakly onto the catalyst surface since significantly high values indicate strong interaction.

460   Table 6 shows the fractional coverage of hydrogen (θ_H), vanillin (θ_{VL}) and vacant site (θ_V) on

461   Pd/C catalyst as a function of time based on equations 9-10 (see Section S1). As reaction time

462   increases the fractional coverage of vanillin decreases while that of hydrogen increases. Hence,

463   consumption of vanillin during the reaction free up space for hydrogen atoms. However, the

464   increase in hydrogen fractional coverage is not as apparent as the decrease in vanillin because of

465   the fixed amount of hydrogen available.

466

467   **Table 6. The Fractional Coverage of VL, H$_2$ and vacant site over time at 328K**.

t(mins)	C_{VL}	θ_V	θ_{VL}	θ_H
10	0.016	0.784	0.136	0.080
20	0.007	0.844	0.070	0.086
30	0.003	0.882	0.029	0.090
40	0.002	0.893	0.015	0.091

468

469   It is worth mentioning that the kinetic data from this study in a batch reactor may need modification

470   for use in a continuous reactor. In a continuous reactor, boundary layers may exist around the

471   catalyst particles thereby subjecting the system to inter particle diffusion limitation, and

472   intraparticle diffusion resistances can occur in the pores of larger particles and pellets. This is not

473   the case in a well-mixed batch system. Hence, this will need to be accounted for in the estimation

474   of Thiele modulus and effectiveness factor.

475   **4. CONCLUSION**

476   In this work, the kinetics of vanillin hydrodeoxygenation reaction was studied in a batch reactor

477   using a commercial 10wt% Pd/C catalyst over the range of conditions: temperature (318 - 338K),

478   hydrogen gas partial pressure (1 – 3MPa), catalyst loading (0.13 – 0.27kg/m^3) and initial vanillin

479   concentrations (35 – 65mM). Preliminary investigation using different agitation speeds (300 -

480   1100rpm) and catalyst particle sizes (80 – 250μm) indicate an absence of external and internal

481   mass transfer resistances for experiments conducted with agitation speed above 900rpm and

482   particles smaller than 250μm. Under this condition, a non-first order reaction kinetics with respect

483   to VL concentration, hydrogen gas partial pressure and catalyst loading was found. The estimated

484   order of reaction with respect to VL concentration lies between -1.2 and -0.7, while the order of

485   reaction with respect to hydrogen gas partial pressure was found to be within the range of 0.14 and

486   0.30. Interestingly, investigation into the effect of products revealed an autocatalytic effect with

487   the reaction enhanced by the presence of either products. In addition, the presence of acetic acid

488   in the reaction environment led to improved vanillin conversion and selectivity towards creosol

489   the desired product. A statistical approach was used to discriminate between competitive

490   dissociative H_2 adsorption model (model I) and non-competitive dissociative H_2 adsorption model

491   (model II). Model I with an R^2 value greater than 99% emerged as the best fit to experimental data.

492   The estimated values from the model were 50.6 kJ/mol for reaction activation energy, 32.5kJ/mol

493   for VL adsorption enthalpy and 28.9 kJ/mol for H_2 adsorption enthalpy.

494

495   **ASSOCIATED CONTENT**

496   Figure S1. SEM micrographs of spent and fresh Pd/C catalyst.

497   Figure S2. Conversion – time and the corresponding rate - time plots due to changes in catalyst

498   loadings.

499   Figure S3. Conversion-time and the corresponding rate-time plots due to changes in H_2 gas

500   partial pressure.

507   DATA

508   Data in this paper is available free of charge via http://edata.bham.ac.uk/

509   AUTHOR INFORMATION

510   **Corresponding Author**

511   * Tel: +44 (0) 121 414 5295. Email: j.wood@bham.ac.uk

522

523 ABBREVIATIONS

524 C_H - concentration of hydrogen in the liquid phase, $kmolm^{-3}$

525 C_{VL0} – initial concentration of vanillin in the liquid phase, $kmolm^{-3}$

526 CR – creosol

527 d_p – catalyst particle diameter, μm

528 D_{ei} – effective diffusivity of species i in equation (i), m^2/s

529 E_A – activation energy of the reaction, kJ/mol

530 H: C – hydrogen to carbon ratio

531 O: C – oxygen to carbon ratio

532 ΔH_H - enthalpy of adsorption for hydrogen, kJ/mol

533 ΔH_{vl} - enthalpy of adsorption for vanillin, kJ/mol

534 HDO – Hydrodeoxygenation

535 K_H – adsorption equilibrium constant for hydrogen gas, $m^3/$ kmol

536 K_S – surface reaction rate constant, $kmol/ (kg_{cat}$ min)

537 K_{Vl} – adsorption equilibrium constant for vanillin, $m^3/kmol$

538 L – Characteristic length of catalyst particle ($d_p/6$)

539 LHHW – Langmuir-Hinshelwood-Hougen –Watson

540   P_H – hydrogen gas partial pressure, MPa

541   r_o – initial reaction rate, kmol/(kg$_{cat}$ min)

542   rpm – revolutions per minute

543   r_{exp} – experimental values of reaction rates, kmol/(kg$_{cat}$ min)

544   r_{mod} – reaction rates predicted from LHHW models, kmol/(kg$_{cat}$ min)

545   R^2 – coefficient of determination

546   RSS – residual sum of squares

547   S_i – active site i on the catalyst surface

548   T – Temperature, K

549   t – Time, minutes

550   VA – Vanillyl Alcohol

551   VL – Vanillin

552   ω – Catalyst loading, kgm^{-3}

553   ϕ – Thiele Modulus

554   η – Effectiveness Factor

555    $\eta\phi_i^2$ – observable modulus for species i in equation (i)

556   X – Percentage conversion of vanillin

557 θ_V – fractional coverage of vacant sites

558 θ_{VL} – fractional coverage of vanillin

559 θ_H – fractional coverage of hydrogen

560 REFERENCES

561 (1) Patel M, Kumar A. Production of renewable diesel through the hydroprocessing of 562 lignocellulosic biomass-derived bio-oil. *Renew Sustain Energy Rev*. **2016**,58,1293–307.

563 (2) Lu M, Du H, Wei B, Zhu J, Li M, Shan Y, et al. Catalytic Hydrodeoxygenation of Guaiacol 564 over Palladium Catalyst on Different Titania Supports. *Energy & Fuels*. **2017**,31,10858–65.

565 (3) Huber GW, Iborra S, Corma A. Synthesis of Transportation Fuels from Biomass: 566 Chemistry, Catalysts, and Engineering. *Chem Rev*. **2006**,106,4044–98.

567 (4) Huber GW, Corma A. Synergies between bio- and oil refineries for the production of fuels 568 from biomass. *Angew Chemie - Int Ed*. **2007**,46, 7184–201.

569 (5) Chheda JN, Huber GW, Dumesic JA. Liquid-phase catalytic processing of biomass- 570 derived oxygenated hydrocarbons to fuels and chemicals. *Angew Chemie - Int Ed*. **2007**, 46, 7164– 571 83.

572 (6) Bridgwater A V. Production of high grade fuels and chemicals from catalytic pyrolysis of 573 biomass. *Catal Today*. **1996**, 29, 285–295.

574 (7) Bridgwater A V. Catalysis in thermal biomass conversion. *Appl Catal A, Gen*. 575 **1994**,116,45–47.

576 (8) Boucher ME, Chaala A, Pakdel H, Roy C. Bio-oils obtained by vacuum pyrolysis of

577 softwood bark as a liquid fuel for gas turbines. Part II: Stability and ageing of bio-oil and its blends

578 with methanol and a pyrolytic aqueous phase. *Biomass and Bioenergy*. **2000**,19,351–361.

579 (9) Bridgwater A V. Review of fast pyrolysis of biomass and product upgrading. *Biomass and*

580 *Bioenergy*. **2012**, 38,68–94.

581 (10) Echeandia S, Pawelec B, Barrio VL, Arias PL, Cambra JF, Loricera C V., et al.

582 Enhancement of phenol hydrodeoxygenation over Pd catalysts supported on mixed HY zeolite and

583 Al_2O_3. An approach to O-removal from bio-oils. *Fuel*. **2014**,117,1061–73.

584 (11) Boullosa-Eiras S, Lødeng R, Bergem H, Stöcker M, Hannevold L, Blekkan EA. Catalytic

585 hydrodeoxygenation (HDO) of phenol over supported molybdenum carbide, nitride, phosphide

586 and oxide catalysts. *Catal Today*. **2014**,223,44–53.

587 (12) Jae J, Tompsett GA, Foster AJ, Hammond KD, Auerbach SM, Lobo RF, et al. Investigation

588 into the shape selectivity of zeolite catalysts for biomass conversion. *J Catal*. **2011**,279,257–268.

589 (13) Li K, Wang R, Chen J. Hydrodeoxygenation of Anisole over Silica-Supported Ni 2 P, MoP,

590 and NiMoP Catalysts. *Energy & Fuels*. **2011**,25,854–863.

591 (14) Mohan D, Pittman CU, Steele PH. Pyrolysis of wood/biomass for bio-oil: A critical review.

592 *Energy and Fuels*. **2006**,20,848–89.

593 (15) Busetto L, Fabbri D, Mazzoni R, Salmi M, Torri C, Zanotti V. Application of the Shvo

594 catalyst in homogeneous hydrogenation of bio-oil obtained from pyrolysis of white poplar: New

595 mild upgrading conditions. *Fuel*. **2011**,90,1197–1207.

596   (16) Fisk CA, Morgan T, Ji Y, Crocker M, Crofcheck C, Lewis SA. Bio-oil upgrading over

597   platinum catalysts using in situ generated hydrogen. *Appl Catal A Gen*. **2009**,358,150–156.

598   (17) Diebold JP, J.P. A review of the chemical and physical mechanisms of the storage stability

599   of fast pyrolysis bio-oils. *NREL*.**1999**.

600   (18) Laurent E, Delmon B. applied catalysis A Study of the hydrodeoxygenation of carbonyl ,

601   carboxylic and guaiacyl groups over sulfided CoMo / y-A1203 and NiMo / 3 / -A1203 catalysts .

602   *Appl Catal A Gen*. **1994**,109,77–96.

603   (19) Pütun E, Uzun BB, Putün AE. Rapid pyrolysis of olive residue. 2. Effect of catalytic

604   upgrading of pyrolysis vapors in a two-stage fixed-bed reactor. *Energy and Fuels*. **2009**,23,2248–

605   2258.

606   (20) Stephanidis S, Nitsos C, Kalogiannis K, Iliopoulou EF, Lappas AA, Triantafyllidis KS.

607   Catalytic upgrading of lignocellulosic biomass pyrolysis vapours: Effect of hydrothermal pre-

608   treatment of biomass. *Catal Today*. **2011**,167,37–45.

609   (21) Choudhary T V., Phillips CB. Renewable fuels via catalytic hydrodeoxygenation. *Appl

610   Catal A Gen*. **2011**,397,1–12.

611   (22) Elliott DC. Historical Developments in Hydroprocessing Bio-oils. *Energy & Fuels*. **2007**

612   ,21,1792–1815.

613   (23) Furimsky E. Catalytic hydrodeoxygenation. *Appl Catal A Gen*. **2000**,199,147–190.

614   (24) Adjaye JD, Reaction C. CATALYTIC CONVERSION OF A BIOMASS-DERIVED OIL

615   TO FUELS AND CHEMICALS I : MODEL COMPOUND STUDIES AND REACTION

616   PATHWAYS. **1995**, 8,131–149.

617 (25) Samolada MC, Baldauf W, Vasalos IA. Production of a bio-gasoline by upgrading biomass

618 flash pyrolysis liquids via hydrogen processing and catalytic cracking. *Fuel*. **1998**,77,1667–1675.

619 (26) Puértolas B, Keller TC, Mitchell S, Pérez-Ramírez J. Deoxygenation of bio-oil over solid

620 base catalysts: From model to realistic feeds. *Appl Catal B Environ*. **2016**,184,77–86.

621 (27) Crossley S, Faria J, Shen M, Resasco DE, Science S, Series N, et al. Solid Nanoparticles

622 that Catalyze Biofuel Upgrade Reactions at the Water / Oil Interface. *Science*. **2010**,327,68–72.

623 (28) Sanna A, Vispute TP, Huber GW. Hydrodeoxygenation of the aqueous fraction of bio-oil

624 with Ru/C and Pt/C catalysts. *Appl Catal B Environ*. **2015**,165,446–456.

625 (29) Wildschut J, Iqbal M, Mahfud FH, Cabrera IM, Venderbosch RH, Heeres HJ. Insights in

626 the hydrotreatment of fast pyrolysis oil using a ruthenium on carbon catalyst. *Energy Environ Sci*.

627 **2010**,3,962–970.

628 (30) Shafaghat H, Sirous Rezaei P, Daud WMAW. Catalytic hydrogenation of phenol, cresol

629 and guaiacol over physically mixed catalysts of Pd/C and zeolite solid acids. *RSC Adv*.

630 **2015**,5,33990–33998.

631 (31) He Z, Wang X. Hydrodeoxygenation of model compounds and catalytic systems for

632 pyrolysis bio-oils upgrading. *Catal Sustain Energy*. **2012**,1.

633 (32) Zhang L, Liu R, Yin R, Mei Y. Upgrading of bio-oil from biomass fast pyrolysis in China:

634 A review. *Renew Sustain Energy Rev*. **2013**,24,66–72.

635 (33) Mortensen PM, Grunwaldt J-D, Jensen PA, Knudsen KG, Jensen AD. A review of catalytic

636 upgrading of bio-oil to engine fuels. *Appl Catal A Gen*. **2011**,407,1–19.

637   (34) Vispute TP, Huber GW. Production of hydrogen, alkanes and polyols by aqueous phase

638   processing of wood-derived pyrolysis oils. *Green Chem.* **2009**,11,1433–1445.

639   (35) Klass D. Thermal Conversion : Pyrolysis and liquefaction. *Biomass Renew energy, fuels,*

640   *Chem.* **1998**,651.

641   (36) Czernik S, Bridgwater A V. Overview of Applications of Biomass Fast Pyrolysis Oil.

642   *Energy & Fuels.* **2004**,18,590–598.

643   (37)   Mahfud FH, Ghijsen F, Heeres HJ. Hydrogenation of fast pyrolyis oil and model

644   compounds in a two-phase aqueous organic system using homogeneous ruthenium catalysts. *J Mol*

645   *Catal A Chem.* **2007**,264,227–236.

646   (38)   Huang F, Li W, Lu Q, Zhu X. Homogeneous Catalytic Hydrogenation of Bio-Oil and

647   Related Model Aldehydes with $RuCl_2(PPh_3)_3$. *Chem Eng Technol.* **2010**,33,2082–2088.

648   (39)   Bindwal AB, Vaidya PD. Reaction kinetics of vanillin hydrogenation in aqueous solutions

649   using a Ru/C catalyst. *Energy and Fuels.* **2014**,28,3357–3362.

650   (40) Sulman A, Mäki-Arvela P, Bomont L, Fedorov V, Alda-Onggar M, Smeds A, et al. Vanillin

651   Hydrodeoxygenation: Kinetic Modelling and Solvent Effect. *Catal Letters.* **2018**,148,1–13.

652   (41)   Maccarrone MJ, Torres GC, Lederhos C, Betti C, Badano JM, Quiroga M, et al. Kinetic

653   Study of the Partial Hydrogenation of 1-Heptyne over Ni and Pd Supported on Alumina.

654   Hydrogenation. **2012**,159–84.

655   (42)   Barták M, Molnár Á. Heterogeneous Catalytic Hydrogenation. PATAI'S Chem Funct

656   Groups. **2009**,2,39698.

657 (43) Bindwal AB, Vaidya PD. Kinetics of aqueous-phase hydrogenation of levoglucosan over

658 Ru/C catalyst. *Ind Eng Chem Res*. **2013**,52,17781–17789.

659 (44) Perego C. Experimental methods in catalytic kinetics. *Catal Today*. **2002**,52,133–145.

660 (45) Weisz PB, Prater CD. Interpretation of Measurements in Experimental Catalysis. *Adv*

661 *Catal*. **1954**,6,143–196.

662 (46) Pintar A, Berčič G, Levec J. Catalytic liquid-phase nitrite reduction: kinetics and catalyst

663 deactivation. *AIChE J*. **1998**;44,2280–2292.

664 (47) CR W, P C. Correlation of diffusion coefficients in dilute solutions. *AIChE J*. **1955**,1,264–

665 270.

666 (48) Wildschut J, Mahfud FH, Venderbosch RH, Heeres HJ. Hydrotreatment of fast pyrolysis

667 oil using heterogeneous noble-metal catalysts. *Ind Eng Chem Res*. **2009**,48,10324–10334.

668 (49) Cheng S, Wei L, Zhao X, Julson J. Application, Deactivation, and Regeneration of

669 Heterogeneous Catalysts in Bio-Oil Upgrading. *Catalysts*. **2016**,6,195.

670 (50) Chen Y, Miller DJ, Jackson JE. Kinetics of aqueous-phase hydrogenation of organic acids

671 and their mixtures over carbon supported ruthenium catalyst. *Ind Eng Chem Res.* **2007**,46,3334–

672 3340.

673 (51) Crezee E, Hoffer BW, Berger RJ, Makkee M, Kapteijn F, Moulijn JA. Three-phase

674 hydrogenation of D-glucose over a carbon supported ruthenium catalyst - Mass transfer and

675 kinetics. *Appl Catal A Gen*. **2003**;25,1–17.

676   (52) Déchamp N, Gamez A, Perrard A, Gallezot P. Kinetics of glucose hydrogenation in a

677   trickle-bed reactor.*Catalysis Today*. **1995**,24.

678   (53) De Bellefon C, Tanchoux N, Caravieilhes S. New reactors and methods for the

679   investigation of homogeneous catalysis. *Journal of Organometallic Chemistry*. **1998**,567.

680

681

682